Wear 566–567 (2025) 205758

Contents lists available at ScienceDirect

Wear

journal homepage: www.elsevier.com/locate/wear

Influencing factors on high temperature tribology

Tobias König [a], Eduard Wolf [a], Philipp Daum [a,b], Dominik Kürten [a], Andreas Kailer [a], Martin Dienwiebel [a,b,*]

[a] Fraunhofer Institute for Mechanics of Materials IWM, Microtribology Center μTC, Wöhlerstr. 11, Freiburg, 79108, Germany
[b] Institute for Applied Materials – Reliablity and Microstructure at the Karlsruhe Institute of Technology, Straße Am Forum 7, Karlsruhe, 76131, Germany

ARTICLE INFO

Keywords:
High temperature
Atmospheric effects
Influence of displacement
Empirical wear correlation
Glaze layer
Wear transition

ABSTRACT

This study investigates the influence of temperatures, normal force, displacement, frequency and sliding distance on the tribological material behaviour of an unlubricated cobalt-based material pairing, as well as the effects resulting from a change of atmosphere from ambient air to a low-oxygen $CO_2/N_2/O_2$-atmosphere. The subsequent identification of empirical wear correlations should enable a transfer to other material systems. Reciprocating wear tests were carried out at up to 800 °C with a cylinder-on-plate contact geometry. The test conditions and the material are based on the application as exhaust gas flap plain bearings for combustion engines.

The temperature has a major influence on the wear behaviour, as it induces the change of tribological mechanisms from abrasion to oxidation and adhesion of wear particles to the formation of a glaze layer in the HT range. The wear particles, required for the tribologically induced sintering process of the glaze layer, are already present in fully oxidised form at low temperatures of 200 °C. The formation of a wear-reducing glaze layer is therefore mainly dependent on the temperature, as this directly influences the sintering process, according to a key finding of this work. The atmospheric influence on the tribological material behaviour is dependent on the temperature related wear regime. For lower temperatures, a mechanism change from abrasion to adhesion takes place in the oxygen-reduced $CO_2/N_2/O_2$-atmosphere. In contrast, the formation of the glaze layer is not influenced by the change in atmosphere. Moreover, the influence of normal force, displacement and sliding distance differs between the various temperature sections and the related tribological mechanisms.

1. Introduction

Nowadays, both the reliability and the maintenance requirements of combustion engines are no longer determined by their mechanical design but rather by the material selection and service life estimation of the parts that undergo wear, corrosion and fatigue. In particular for larger engines used for marine, train or off-highway applications, where unplanned downtimes lead to very high costs, degradation of the mechanical function is under particular attention. Critical tribological systems are mainly found in the exhaust gas systems of these engines, since liquid lubricants cannot be used at temperatures above 400–500 °C and unlubricated friction leads to high wear rates [1]. The latest, very restrictive emission specifications have led to a significant increase in the control and regulation effort in the exhaust gas systems, resulting in a high number of tribological contacts in the exhaust line, e.g. in flap or control systems.

In order to achieve sufficiently long lifetimes and long maintenance intervals, high alloyed and wear-resistant cobalt base materials are used for these components. Regarding the changed requirements for both, materials and combustion systems, exact knowledge and predictability of the wear behaviour and its influencing factors are necessary for the reliable calculation of maintenance intervals.

According to Blau [2], research on the wear of metals has improved dramatically over the last 50 years thanks to the use of high-precision testing equipment and, above all, the development of advanced analytical methods, enabling a detailed understanding of occurring wear processes. Several publications have already investigated the wear behaviour of cobalt alloys [3–9]. Renz et al. focused on the application in valves, Dreano et al. investigated fretting between the guide vanes and the turbine shaft, do Nascimento et al. analysed the abrasive wear properties of Co oxides, McCarron et al. dealt with the application in nuclear power plants and Cross et al. conducted model tests at room temperature with a reciprocating mode of motion. It is questionable how far these results can be transferred to the application in plain bearings, which are exposed to high thermal loads but also chang-

* Corresponding author.
E-mail addresses: tobias.koenig@iwm.fraunhofer.de (T. König), martin.dienwiebel@kit.edu (M. Dienwiebel).

https://doi.org/10.1016/j.wear.2025.205758
Received 17 June 2024; Received in revised form 13 December 2024; Accepted 20 January 2025
Available online 25 January 2025

ing atmospheres in the exhaust gas system and experience oscillating motion.

In addition to an experimental verification of the material and load-dependent wear behaviour, it can also be estimated using a generally valid wear model. The widely used and simple wear equation by Archard [10] shows a linear correlation between the wear volume and the normal force as well as the sliding distance, but the important influence of temperature is not taken into account. For high-temperature applications, Quinn [11] extended this equation and correlated the wear behaviour with the oxidation properties of the materials. By taking into account an Arrhenius equation for the temperature dependence of wear, the wear increases exponentially with higher temperatures. A major disadvantage of this model description by Quinn is the precise determination of the required coefficients. Jiang/Stott et al. [12,13] took a different approach, developing a particle-based, temperature-dependent model based on the significant influence of particles on wear behaviour. This model is able to calculate the formation of a thick, wear-reducing particle layer and that of a glaze layer. A glaze layer is a friction- and wear-reducing, tribologically induced third body that is created by compacting and sintering of oxidised wear particles and is named in this way because of its shiny surface. The Jiang/Stott wear model is very complex, as the load- and atmosphere-dependent particle generation (number, size), their transport, ejection, agglomeration and sintering, as well as their effects on wear, must be taken into account. Consequently, it is not suitable for simply estimating the effects of different load conditions on the wear behaviour and a high level of experimental effort is required to adapt it to a particular material pairing. Furthermore, as soon as the glaze layer is formed, this model assumes that no additional wear will occur, which is not very realistic. A new wear model for a co-alloy from Dreano [4,6], which is based on the model from Quinn, was adapted to the operating conditions and influencing factors at fretting. Again, no additional wear is assumed as soon as the glaze layer is formed. However, it is questionable whether and to what extent this model can also be applied to plain bearings and their influences. To summarise, there are no experimental wear results for a Co alloy as an unlubricated high-temperature plain bearing, nor can an existing wear model be simply and reliably transferred to this application with the particular material system.

The aim of this publication is to identify the influences of important operating parameter on the wear behaviour and to determine the effects on the dominant tribological mechanisms. Finally, the understanding of the interactions between the mechanisms and the wear-determining influencing factors should be extended. In order to enable the transferability of these results to other material systems, mathematical correlations between the influencing factors and the wear values should also be determined instead of developing a complex wear model that only describes the wear behaviour of the investigated material pairing.

Consequently, the influences of temperature, normal force, displacement, sliding distance or time as well as atmosphere on the tribological material behaviour were investigated. The influence of higher speeds has already been investigated many times and can mainly be reduced to a local friction-induced temperature increase [14–16]. The influence of the atmosphere has also been investigated many times, but either for other gas compositions [17–19] or other material systems [13]. In contrast, this publication focuses explicitly on the plain bearing application in exhaust gas systems of internal combustion engines, therefore, as in [20], a reversing model test with line contact geometry and atmospheres that are intended to simulate the diesel exhaust gas were used.

2. Materials and methods

2.1. Materials

For this study, a cobalt-based material pairing was investigated, consisting of a cast cylinder out of CoMo28Cr8Si2 (Tribaloy® T400) and a high velocity oxygen fuel (HVOF) sprayed CoMo28Cr17Si3 (Tribaloy® T800) plating of a ferritic heat resistant steel plate (1.4713). The composition of these materials is listed in Table 1. As the steel base material of the plate does not influence the tribological behaviour, a detailed description and analysis of this material is not included.

Table 1
Composition of the studied materials in w.% [22,23].

Material	Co	Cr	Mo	C	Si	Others
CoMo28Cr8Si2 cast cylinder	base	8.5	28.5	<0.1	2.6	Ni, Fe
CoMo28Cr17Si3 HVOF on plate	base	17.5	28.5	<0.1	3.5	Ni, Fe

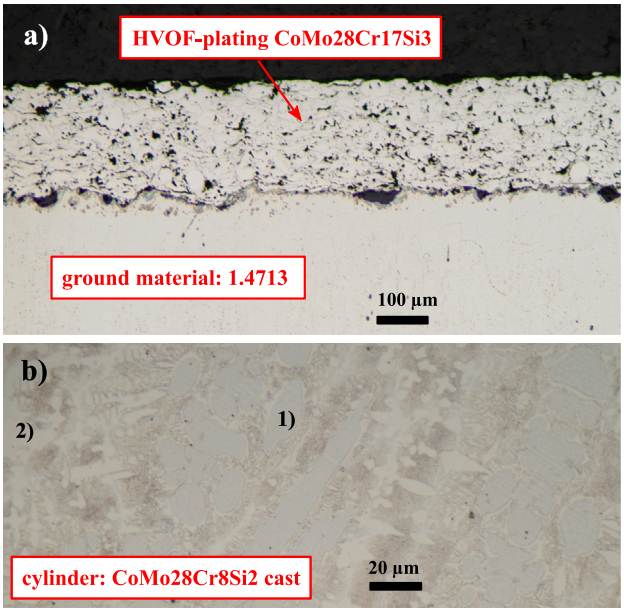

Fig. 1. Metallographic micro-sections of the studied materials: (a) Plate: around 200 µm thick HVOF-plating CoMo28Cr17Si3 on 1.4713; (b) Cylinder: cast CoMo28Cr8Si2 with (1) primary Laves phase with low Cr and (2) Co solid solution with eutectic structure [21].

The microstructure of the cast cylinder consists of a primary Laves phase with low Cr amount and a Co solid solution with a eutectic structure (Fig. 1 b) [21]. The identification of the microstructure with established analytical methods was not possible for the 200 µm thick HVOF-sprayed CoMo28Cr17Si3 plating, but the porous structure of the plating with voids of 10 µm in diameter and the deformed particle boundaries were observed (Fig. 1 a).

2.2. Tribological experiment

An oscillating sliding test rig (SRV IV®, Optimol Instruments, Germany) featuring a recently developed cylinder-on-plate contact configuration (Fig. 2b), which is described elsewhere [20] in detail, was used to conduct reciprocating wear tests. This configuration allowed a low initial mean Hertzian pressure of 175 MPa at a normal load of 50 N. The upper cylinder, shown in orange, is 15 mm long and has an 8 mm diameter. It can be adjusted via rotation around an axis in the direction of sliding (axis: green arrow in Fig. 2), to achieve a line contact with the plate throughout its entire length. The plate is fixed directly into a heated bracket and measures 24 mm in diameter and 7.9 mm in height. A thermocouple was soldered to the surface of every plate and utilised to regulate the heating in order to precisely determine the test temperatures. Two additional radiation heaters were used for tests at 800 °C.

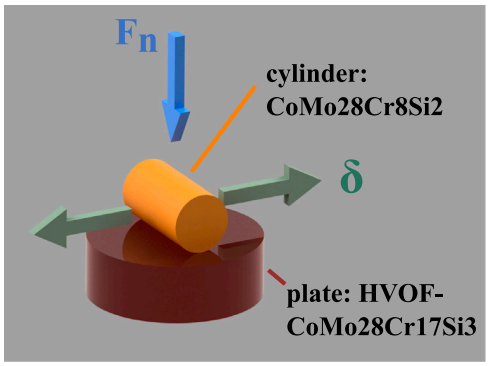

Fig. 2. Contact geometry with normal force F_n (blue) and displacement δ (green): Lying cylinder on plate.

To conduct tribological tests in a defined exhaust gas like atmosphere, the same setting of [20] was utilised: A gas mixture of 20 vol.% CO_2 and 80 vol.% N_2 (BIOGON® C20) was directly introduced into the chamber of the test rig. The gas flow was controlled and regulated to a predefined oxygen amount, which was measured by a heat resistant oxygen sensor (Bosch LSU 4.9) positioned close to the contact bodies. In the case of 5 vol.% O_2 and a mix of ideal gases, the amount of CO_2 that results in the test chamber is 15.2 vol.%, assuming that the inflow gas mixes with air as leakage. To create a uniform gas mixture, an additional fan was put into the test chamber.

Two shear sensors (Kistler Z21654A2) and a dedicated charge amplifier (Kistler 5018) were used to measure the friction force. This force measurement system was verified using calibration weights, pulleys, and a cable pull. Three alternating force tests up to ±100 N were conducted, and a maximum deviation of 1.02 N was attained. A recording rate of 5 kHz was used to constantly capture the force and position signal from the test rig. The dissipated energy of one friction cycle (E_d) was then divided by four times the normal force (P) multiplied by the sliding amplitude (δ_0) to determine the energetic coefficient of friction ($ECoF$) [24]:

$$ECoF = \frac{E_d}{4\ P\ \delta_0} \tag{1}$$

This calculation technique is used to effectively limit the impact of wear-scar interaction on the coefficient of friction and to enable comparison of the results with those of other tribological tests, as demonstrated elsewhere [25–27]. Furthermore, the American Society for Testing and Materials approved the calculation as a standard [28].

Also the test preparation and execution of [20] was applied: The samples were thoroughly cleaned with isopropanol to eliminate any finishing process residue before the tribological tests. After mounting and adjusting the samples in the test rig, they were heated to the appropriate temperature and left there for at least twenty minutes in order to create a uniform distribution of heat. Gas intake and regulation for the CO_2 atmosphere tests were initiated prior to sample heating and terminated when the temperature dropped below 100 °C.

Table 2 lists the standard test parameters of this research, which are identical to prior studies of [20]. Modified parameters were used to analyse the influence of the normal force and the displacement; these are mentioned in the corresponding subsections. Typically, a test was repeated three times, which is indicated by a scatter bar in the resulting diagrams. If no scatter bar is presented, the test was only performed once.

Table 2
Standard test parameters of the tribological experiments.

Parameter	Value	Unit
Load	50	N
Displacement	1.6	mm
Frequency	15	Hz
Duration	120	min
Temperature	RT - 800	°C
Atmosphere	Ambient air, CO_2-N_2-mixture with ambient air and resulting 5 vol.% O_2	–

2.3. Characterisation methods

For the microstructural analyses, the microsections were etched with Beraha I for 1.5 minutes and investigated and imaged using an optical microscope.

The same wear measuring procedure of [20] was conducted to achieve a comparability of the tribological results: For both contacting bodies, the wear volume was measured using a confocal microscope with an integrated structured illumination technique. Only the centre of the contact region was captured with a width of 633 µm to measure the sample height at a resolution of 0.2 µm. A reference height was identified at the tribologically untreated area in the following evaluation process, and the wear volume and transfer were calculated and extrapolated for the entire contact body.

A scanning electron microscope (SEM) with a secondary electron detector was used to further analyse the tribological test specimen with the objective to identify the main wear mechanisms. An acceleration voltage of 8 kV and a working distance of about 8 mm was used for recording surface images. Focused ion beam (FIB) in combination with the SEM was utilised to analyse adhering particles and material transfer in detail with a Helios 650 Dual Beam instrument (Thermo Fisher Scientific, Waltham, MA, USA). The surface was protected from ion beam damage at high currents during the cross-sectioning process by the use of ion beam aided deposition of a platinum-containing layer.

To study the tribochemical changes that are related to thermal and atmospheric effects, X-ray photoelectron spectroscopy (XPS) was applied for selected samples after the tribological tests and cleaning with cyclohexane and isopropanol. XP spectra were obtained with monochromatic Al Kα (1486.7 eV) X-rays using a PHI 5000 VersaProbe™ II (Physical Electronics Inc). Applying a 200 µm spot size, element spectra of the surface were measured with an energy precision of 0.1 eV and a pass energy of 23 eV. Depth profiles of the constituent elements were measured with the same spot size, utilising argon ion sputtering, an energy resolution of 0.2 eV, and a pass energy of 47 eV. Using a SiO_2 wafer with a predetermined surface thickness, the depth scale was calibrated. Selected samples were typically sputtered for 25 minutes at a rate of 2 nm/min (500 nA, 1 kV) to acquire a detailed view of the chemical composition at the surface. Subsequently, the sputter rate was increased to 10 nm/min (2000 nA, 2 kV) for the next 45 minutes, resulting in an overall profile depth of 500 nm. Analysing XP spectra and depth profiles with LLS fitting was done using the PHI-Multipak software.

Furthermore, individual wear particles were examined after the tribological test using transmission electron microscopy (TEM) in order to determine their shape, size, structure and chemical composition. Therefore, the wear particles after the test were flushed down from mainly the plates with ethanol and were stored and transported in this liquid. Afterwards, the dispersion of powder was brought onto a holey-carbon film on a Cu-grid as a sample carrier. HAADF-STEM and EDS/EELS was used to investigate the chemistry and morphology of the sample states. The experiments were performed on an FEI Titan microscope using an CS-corrector at 300 keV electron energy, including EELS spectrometer. The data were converted and analysed with the FEI software package "TEM imaging and analysis" (TIA) version 4.7 SP3 and with "Gatan Digital Micrograph 3.53".

3. Results and discussion

In this study, several factors influencing the high temperature wear behaviour of unlubricated metal contacts were investigated. These results and the corresponding discussion are divided into five sections in order to clearly distinguish the individual effects.

3.1. Influence of temperature

The mean energetic coefficient of friction ($ECoF$) of individual tests at different temperatures, as well as the mean wear volume of plate and cylinder are shown in Fig. 3. If scatter bars representing the standard deviation are shown, three independent tests were performed. If not, the test was not repeated. For low temperatures of room temperature (RT) and 100 °C minimal wear took place, and intermediate friction between 0.6 and 0.7 was measured. In this temperature regime, mainly the cylinder was worn, the wear of the plate stayed at a low level and the intermediate friction behaviour was constant over the test duration. With intermediate temperatures of 400–500 °C the wear behaviour drastically changed, the wear of the cylinder decreased, and the wear of the plate reached the highest values of this material pairing. Moreover, at 500 °C the friction started to increase to 0.7. The second dominant change of the wear behaviour was measured at the high temperature section between 600–800 °C, where wear of cylinder and plate drop to minimal values. The friction behaviour showed this transition with slightly shifted temperatures. At 600 °C the increasing trend of 500 °C was followed, resulting at the highest friction of 0.86, whereas at 700–800 °C the lowest friction values of 0.34 were recorded. Particularly at these two highest temperatures, a running-in behaviour in the first 15–20 minutes was measured, for lower temperatures a mainly constant friction over time was observed.

To clarify the main dominating wear mechanisms of these temperature sections, the worn surfaces of the cylinders and plates, tested at 200, 400, 600 and 800 °C were displayed in Figs. 4 and 6, respectively. For 200 °C, a flattened, abrasively worn contact region on the cylinder was visible, the corresponding plate surface showed just slight abrasive marks. These characteristics are specific for the contact bodies tested up to 300 °C and correlate the higher wear of the cylinder and intermediate friction. For the temperature section of 400–500 °C aside from light abrasive grooves, a lot of wear particles adhered on the cylinder, forming flakes. The plate shows corresponding grooves and a high amount of debris was found beside the contact area on the samples. Whereas the specimen tested at 600–800 °C show completely different wear characteristics for both contact bodies. A smooth and shiny surface, almost polished was found on the cylinders, only the plate tested at 800 °C differs, showing a partly formed, lighter surface layer. On the cylinder tested at 600 °C just a few abrasive grooves can be recognised, but with increasing temperature their amount increases clearly. This difference in the grooving is even more evident in Fig. 5, which contrasts two height sections of the cylinder wear surfaces. The mentioned wear surface characteristics together with the low wear and friction amount indicate that a shear-induced glaze layer has developed. This favourable high temperature wear behaviour was already reported by [6] for fretting with other cobalt-based material pairings. For the lowest temperature range (RT-300 °C) a dominant abrasion of the cylinder with intermediate friction is observed and for the intermediate temperature range (400–500 °C), a wear-reducing third body forms due to the adhesion of wear particles on the cylinder and results in high wear of the plate and rising friction.

The element concentration of XPS analysis in a depth of 500 nm for different test temperatures is displayed in Fig. 7 to clarify the thermal effect on the material composition. The underlying depth profiles are included in the supplementary data for more detailed studies. At room temperature, the measured compositions of plate and cylinder are comparable to the ground material composition listed in Table 1, that reveal a low tribochemical influence. The minimal amount of oxygen

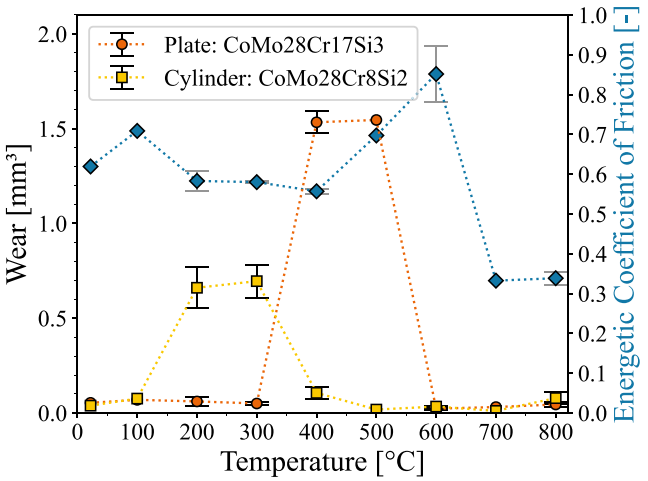

Fig. 3. Tribological results of isothermal tests in air (50 N, 15 Hz, 1.6 mm & 120 min).

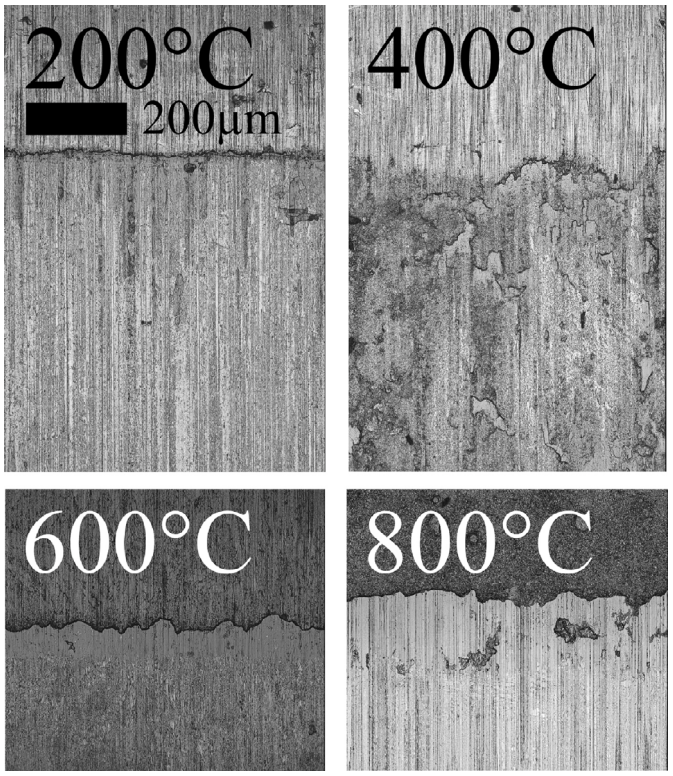

Fig. 4. Worn surface details of cylinders (CoMo28Cr8Si2 cast) after isothermal tests in air (50 N, 15 Hz, 1.6 mm & 120 min); all images have the same scale, showing the worn area in the lower section.

at the plate, slightly decreasing over the measurement depth of 1 µm is correlated to the HVOF process during manufacturing. But already at 200 °C a slight amount of oxygen in a depth of 500 nm was determined and the other elements start to decrease. This is accompanied by a 100 - 200 µm thick oxygen rich surface layer, which can be seen in the depth profiles. The results of 400 °C do not quite match the almost linear trends of the elements, but mark switching points for mainly the cylinder. The oxygen amount of the cylinder is significantly higher and deeper than at 200 °C and also the cobalt content dropped. This feature can be correlated with the distinct change in wear behaviour and the high amount of adhering wear particles on the cylinder, forming a third body and wear the plate. For the higher temperatures of 600 and 800 °C a high amount of oxygen was observed accompanied by a nearly

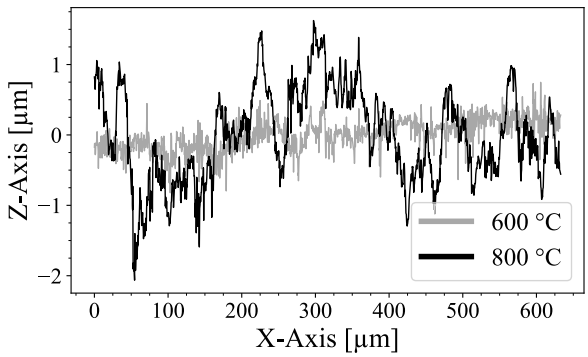

Fig. 5. Representative height section of cylinders' wear scar (CoMo28Cr8Si2 cast) after isothermal tests at 600 & 800 °C in air (50 N, 15 Hz, 1.6 mm, 120 min); X-Axis perpendicular to the direction of movement.

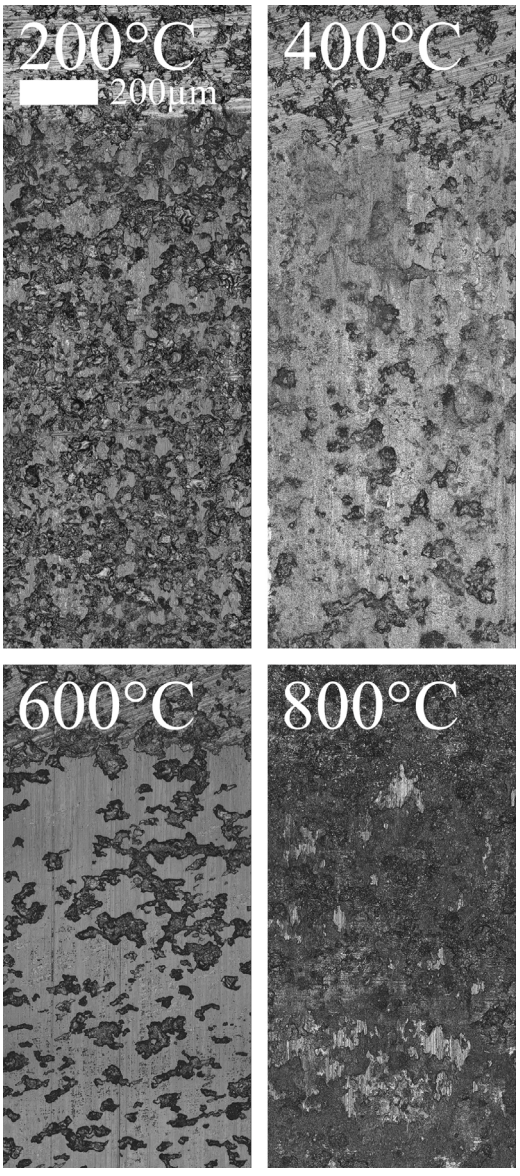

Fig. 6. Worn surface details of plates (CoMo28Cr17Si3 HVOF-plating) after isothermal tests in air (50 N, 15 Hz, 1.6 mm & 120 min); all images have the same scale and show the worn area in the lower section.

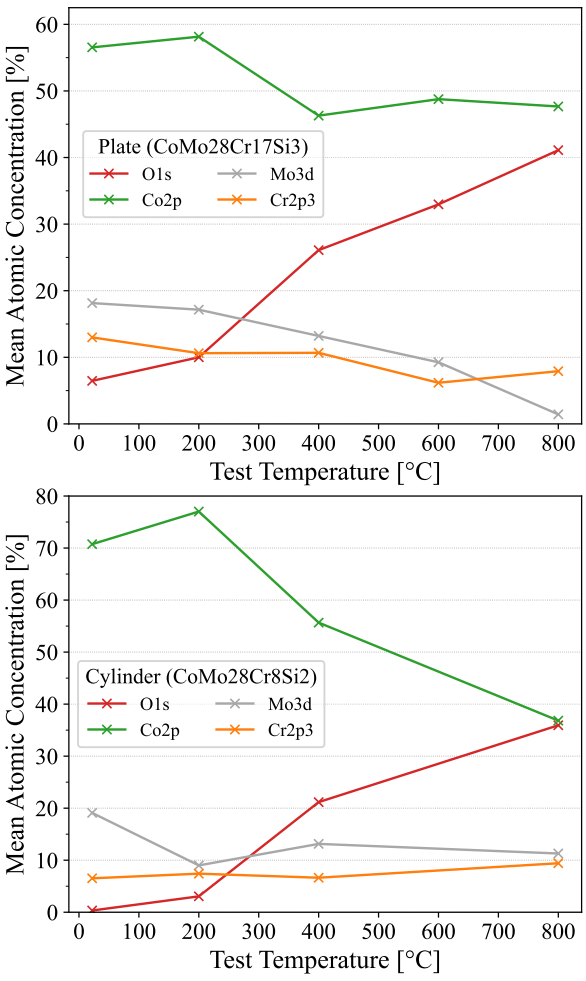

Fig. 7. Element concentration of XPS depth profiles at 500 nm over temperature for plates and cylinder tested in air (50 N, 15 Hz, 1.6 mm & 120 min).

homogeneous trend of the deep profiles, which indicates a thick oxidic surface structure, that was formed within the tribological contact.

The specific chemical composition and especially the oxidation state of cobalt could neither be identified by Raman spectroscopy due to a laser-induced transition of the oxide states [29], nor by the XPS results due to comparable binding energies of the Co2p peak for different oxides. However, it is assumed that at temperatures above 600 °C a glaze layer structure similar to that described by [5] is formed, which has a strong effect on the friction and wear behaviour. It must be emphasised that at 600 °C a significantly higher friction was measured, compared to the higher temperatures, but the wear reducing properties of the glaze layer were already observed. This phenomenon of high friction and low wear in the lower temperature range of a Co-based glaze layer was also demonstrated by Dreano et al. [30]. There, the high coefficient of friction was attributed to an increased amount of Cr_2O_3 in the glaze layer composition. This correlation cannot be confirmed with the determined XPS results (Fig. 7). Instead, a difference was determined between the oxygen contents at 600 and 800 °C, which indicates a change of the oxidation state. The strong influence of different oxides on dry friction was also demonstrated by [31,32], suggesting this to be the cause of the different friction levels. As previously discussed, it was not possible to determine the specific chemical compositions and oxidation states with certainty using the measured XPS results and Raman spectroscopy.

To investigate the formation process of the glaze layer, which is widely postulated as a tribologically aided sinter process of oxidised,

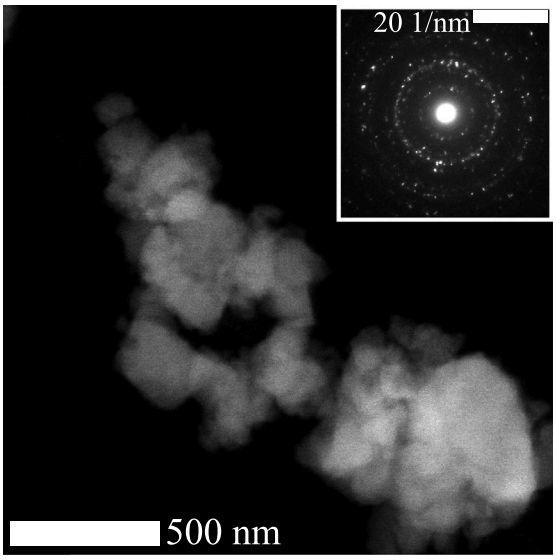

Fig. 8. High-angle annular dark field (HAADF) TEM image and selected area diffraction of a wear particle generated in a tribological test at 200 °C in air.

Table 3
Elemental quantification (EELS) of a wear particle generated at a tribological test at 200 °C in air.

Element	Shell	Composition (at.%)
C	K	16.2
O	K	44.6
Cr	L	11.4
Mn	L	0.12
Co	L	27.6

agglomerated and compacted wear particles, debris of different test temperatures were analysed by TEM.

In Fig. 8 a high-angle annular dark field (HAADF) TEM-analysis of wear particles generated at 200 °C is shown. At first the high contrast between the particles and the sample carrier has to be mentioned, which results by a high atomic number difference or a high thickness and density of the particles. Secondly the different particle sizes, between several μm and some 100 nm were observed. Thirdly, by the investigation of the selected area diffraction (SADP), a poly/nanocrystalline structure was concluded due to the sharp reflections. As a next step, the chemical composition was investigated with electron energy loss spectroscopy (EELS). The identified elemental quantities are summarised and listed in Table 3. The wear particles mainly consist of cobalt, chromium and oxygen, the amount of carbon is attributed to the sample carrier and the solution in ethanol for transportation and storing. Assuming that the amount of cobalt is present as fully oxidised CoO and the amount of chromium is present as Cr_2O_3 the corresponding oxygen fraction would be 44.7 at.%. This fraction agrees with the measured oxygen fraction of 44,6 at.%, which of course underlies some uncertainty. It can be deduced, that the analysed wear particles have a chemical composition that matches mainly CoO, Cr_2O_3 and a small amount of manganese. In a subsequent energy dispersive X-ray (EDX) analysis, the mapping of the elements within the wear particles was investigated. The results, which can be found in the supplementary data, reveal a good co-location of the oxygen with the metals and thus a homogeneous element distribution and no concentration gradient is concluded.

The same analytical methods were used to investigate the properties of wear particles, that were generated in a tribological test at 600 °C, where a wear reducing glaze layer was formed. The HAADF analysis in Fig. 9 indicates a comparable particle size and contrast to the results of 200 °C. Also, a poly/nanocrystalline structure can be deduced by

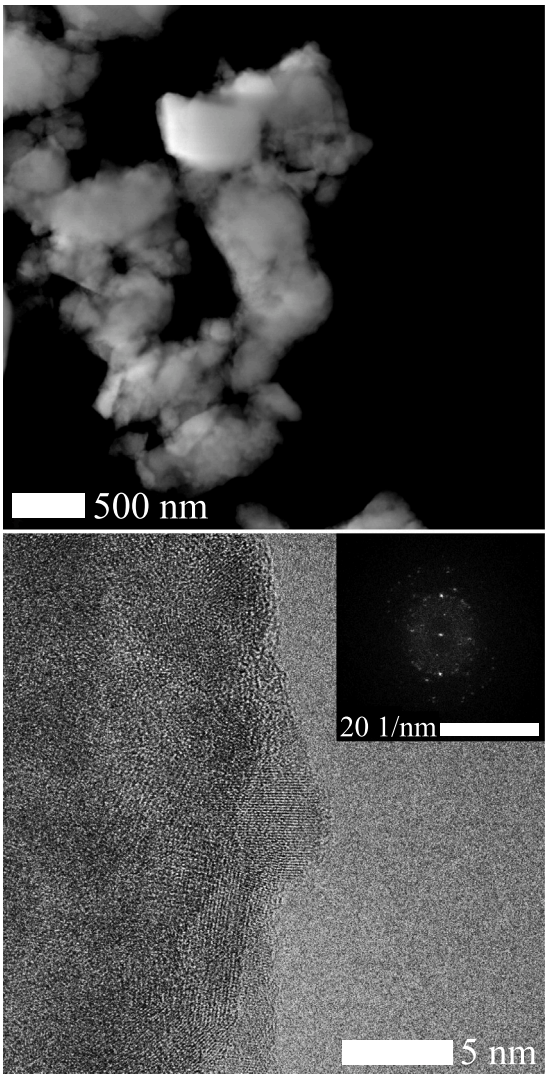

Fig. 9. High-angle annular dark-field (HAADF) image (upper), high resolution TEM and selected area diffraction (lower) of a wear particle generated in a tribological test at 600 °C in air.

sharp reflections in the SADP. Moreover the nanocrystalline structure with grain sizes smaller than 10 nm was proven by a high resolution TEM-picture, displayed in Fig. 9. In Table 4 the chemical composition measured by EELS is listed. The measured particles mainly consist of cobalt, chromium and molybdenum. With the same assumption like before, that the metal oxides CoO, Cr_2O_3 and MoO_3 are formed, a corresponding oxygen fraction of 31.9 at.% is needed. This calculated oxygen fraction agrees with the measured one of 33.9 at.%. Furthermore, the EDX maps confirm a homogeneous element distribution within the particles (see supplementary data). It therefore can be concluded that the investigated particles of tribological tests at 200 and 600 °C neither differ in the chemical composition, nor in the structure or element distribution.

These results of the wear particle analysis are important to understand the formation process of the glaze layer. The tribologically enhanced sintering of oxidised wear particles in the contact zone is the dominant process for the formation, as many recent publications agree [5,6,33–36]. Sinter processes are generally based on grain boundary and lattice diffusion, as they are the dominant mechanisms for densification [37]. The diffusion itself is dependent on the material, temperature and the time. However, the particle size also determines the sintering speed, as the reduction of the free surface and thus the

Table 4
Elemental quantification (EELS) of a wear particle generated at a tribological test at 600 °C in air.

Element	Shell	Composition (at.%)
Mo	M	0.75
C	K	39.1
O	K	33.9
Cr	L	6.8
Co	L	19.4

free energy of the system is the driving force for sintering [37]. This generally accepted relationship has also been specifically investigated for tribologically induced sintering processes by [38], and a faster formation of the glaze layer when smaller oxide particles are added has been demonstrated. The last factor influencing the sintering speed is the compressive stress, which also contributes to the reduction of the system's free energy and acts as a driving force for the sintering process [37]. Since both the compressive stress and the particle size determine the reduction of the free surface or free energy, the compressive stress is less effective in promoting the densification of finer particles [39]. To summarise, the material, temperature, time, particle size and the compressive stress are the factors influencing the sintering speed.

Based on the previous analyses, it was demonstrated clearly that both the oxide state and the nanocrystalline structure of the wear particles do not differ between experiments at 200 and 600 °C. Nevertheless, a wear reducing glaze layer formation was observed only at 600 °C. Since the same test durations and normal forces were used for the tests, these parameters can be excluded as dominant factors of the sintering process. This means that only the temperature and particle size possibly differ between the tests and are responsible for the formation of the glaze layer. Since the distribution of particle sizes ranges from a few µm to 100 nm and thus covers the entire size range tested by [38], it is assumed that the particle size is not the dominant factor influencing the sintering process of a glaze layer. Nevertheless, further particle analyses should be carried out in the future in order to clarify the temperature-dependent particle size distributions and to support this hypothesis. However, it should be highlighted that the temperature is considered to be a decisive influencing factor in the sintering process, which is responsible for the formation and continuous regeneration of a glaze layer.

To mathematically define the temperature influence on the wear behaviour of the tested material combination, the following abrasive-oxidative description based on [4] and [11] can be used for the lower temperature range including 500 °C, which is characterised by abrasion and the adhesion of oxidised wear particles:

$$V_T \sim e^{-\frac{E_a}{RT}}$$
$$\text{with} \quad E_{a,I} \quad \text{for} \quad T < T_{GL} \qquad (2)$$
$$\text{and} \quad E_{a,II} \quad \text{for} \quad T > T_{GL}$$

Here E_a stands for the activation energy of the tribologically enhanced oxidation, R is the universal gas constant, T is the mean temperature of the specimen and T_{GL} is the temperature threshold for the glaze layer formation, representing an Arrhenius equation.

Above a certain temperature threshold T_{GL}, which is between 500 and 600 °C for this material system in this test arrangement, the thermally activated sintering process of the oxidised wear particles sets in. This results in the formation of a glaze layer. Due to the retention of the debris in the contact zone, formation of a load bearing surface layer and the continuous regeneration of this layer after disruptions, the wear of the tribological system decreases significantly, comparable to other studies [6,33,34,40]. The glaze layer formation is accompanied by a significant friction drop. Having a closer look at the wear results at 600 to 800 °C in Fig. 3, a slight increase of wear with temperature can be observed. This correlates with a significant increase of abrasive

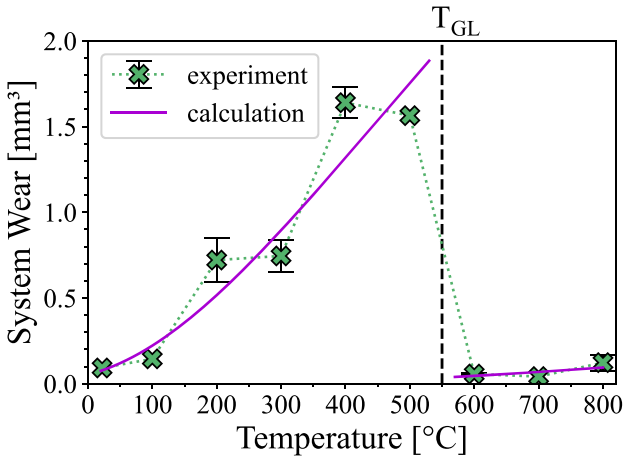

Fig. 10. Tribological results of isothermal tests in air (50 N, 15 Hz, 1.6 mm & 120 min) and with Eq. (2) calculated temperature dependent wear volume.

Table 5
Determined mathematical model parameter.

Parameter	Value	Unit
$E_{a,I}$	12.39	kJ/mol
$k_{T,I}$	12.052	mm³
$E_{a,II}$	28.510	kJ/mol
$k_{T,II}$	2.294	mm³

grooves in the glaze layer surface. Therefore, a thermal stability range is proposed for the investigated glaze layer which allows the wear behaviour in the high temperature range to also be described with an Arrhenius relationship. Following this, the wear volume for the whole temperature range can be described by Eq. (2) but different magnitudes and activation energies below and above T_{GL} have to be considered.

The pre-factors and activation energies listed in Table 5 are calculated for the investigated material system. Fig. 10 compares the measured wear values with the calculated ones. Of course, such a simple mathematical description does not reflect the complex interactions in the tribological system, which lead to different wear values of the contact bodies and the step-like increase in wear with temperature. Nevertheless, this description can be used to roughly estimate the wear to be expected in the case of a temperature change.

Furthermore, a thermally induced phase transition of the base materials as an influencing factor on the wear behaviour is excluded based on the results of Xu et al. [41]. They demonstrated the first thermally induced phase transition at a temperature of 1338.2 °C for CoMo28Cr8Si2, at which both microstructural fractions, namely the Laves phase and the co-solid solution, simultaneously transform into melt. They also showed that the melting point increases with a higher Laves phase content, which means a higher melting temperature can be expected for the higher alloyed CoMo28Cr17Si3 material. In addition, Peng et al. [42] determined a preferential oxidation of the Laves phase at 900 °C as part of their oxidation studies on both materials. This preferential oxidation was proven with microsections of worn samples, tested at 800 °C, which were shown in the supplementary data. However, if a thermally induced phase transition would already occur at these temperatures, such a conclusion would no longer be possible due to the mixing of the microstructural fractions. It is therefore sufficient to focus on the processes near the surface during tribological loading, such as oxidation, particle formation etc. up to the formation of a glaze layer, as no phase transition of the base material takes place in the temperature range investigated.

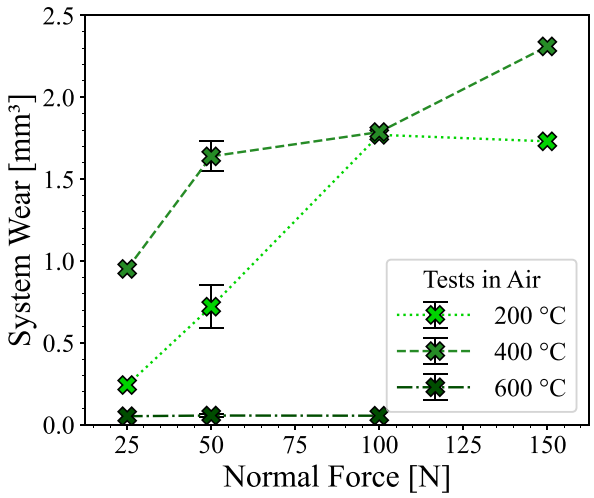

Fig. 11. Wear results of isothermal tests in air at different normal forces (15 Hz, 1.6 mm & 120 min).

3.2. Influence of normal force

The normal force is the next important influencing factor, which was investigated. To distinguish between the effects on the low temperature behaviour, which is characterised by abrasion and oxidation, and the high temperature behaviour with glaze layer formation, the normal forces were varied at 200, 400 and 600 °C. The corresponding wear volumes of both samples are summarised as system wear to highlight the trends, which are shown in Fig. 11.

For the two lower temperatures, a nearly linear increase of the total wear of both contact bodies with rising normal force was observed. Consequently, the wear volume dependency on the normal force P below T_{GL} can be mathematically described as linear correlation:

$$V_P \sim P \qquad \text{for} \quad T < T_{GL} \tag{3}$$

This correlation for unlubricated material pairings was found by several researchers [4,43], finds application in wear equations of Archard and Quinn [10,11] and is correlated with adhesive and abrasive wear regimes.

In the temperature range of the glaze layer formation, the wear volumes do not differ between different normal forces. Consequently no proportionality between the normal force and the wear volume above T_{GL} can be concluded:

$$V_P \nsim P \qquad \text{for} \quad T > T_{GL} \tag{4}$$

This result is in contrast to Kato [44], who identified a strong correlation between the applied normal force and the sliding distance, which is needed to form a glaze layer out of the oxide particles previously placed in the friction track. The main differences to the present results is seen in the time and wear volume needed for the generation of these particles and the lower particle ejection of a continuous running pin-on-disc-test compared to the reciprocating model test, which was used here. The tribological system investigated here initially has to generate a sufficient number of oxidised wear particles to form a wear-reducing glaze layer and to compensate the particles, which are ejected out of the tribological contact by the movement of the specimen. This number is comparable for the applied normal forces, so that no normal force influence was identified.

3.3. Influence of displacement/frequency

The influence of higher frequencies and consequently higher sliding velocities on the tribological behaviour of unlubricated contact pairings has already been investigated in many cases. For example, Stott distinguishes in [12] between high-speed sliding and medium sliding speeds of approx. 100 mm/s and points out the different local friction-induced temperature increase, which leads to strong oxidation at high speeds. Jin et al. showed for fretting a strong correlation between the glaze layer formation and the frequency [15] in addition to the temperature dependence. This complex interaction was also demonstrated by Zhang et al. and visualised in illustrative mechanism maps [16]. Consequently, this interaction is considered as understood and was not investigated further.

The aim of the following investigations was to determine the influence of different oxidation times as well as the underlying mechanism on the wear behaviour resulting from frequency variations and the recurring traversing of the contact bodies during reciprocating experiments. For this purpose, three different frequency-displacement combinations were selected, which have a comparable average speed and consequently comparable friction-induced local temperature increases. Furthermore, identical total sliding distances were selected in order to introduce the same friction energies into the tribological systems. These parameter combinations are summarised in Table 6.

Table 6
Test parameter combinations to investigate the displacement and frequency influence.

Nr. –	Freq. [Hz]	Displ. [mm]	Av. speed [mm/s]	Duration [h]	Distance [m]	Cycles [10^3]
A	8	3.2	51.2	1.875	345.6	54
B	15	1.6	48	2	345.6	108
C	30	0.8	48	2	345.6	216

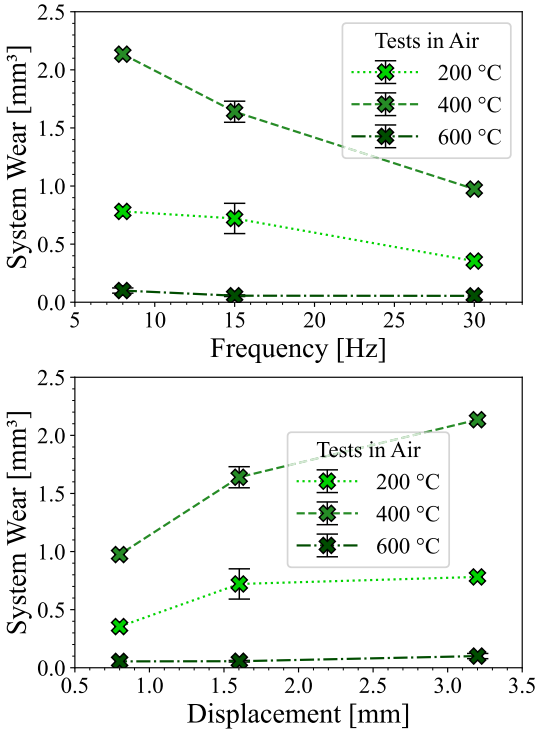

Fig. 12. System wear in air for selected temperatures over frequency and displacement (50 N, 8 Hz/3.2 mm, 15 Hz/1.6 mm, 30 Hz/0.8 mm, 345 m).

The measured wear results are shown in Fig. 12 as a function of the frequency and the displacement. Especially for the low temperature range, which is dominated by abrasion and oxidation, a significant decrease in the wear volume with increasing frequency can be observed. However, for 600 °C, which corresponds to the glaze layer regime, only a minimal decrease in wear with increasing frequency was demonstrated.

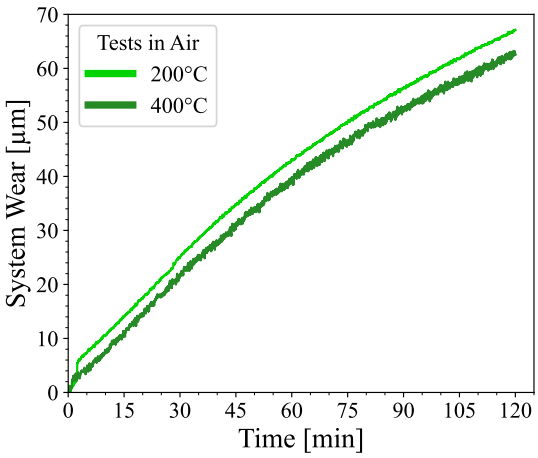

Fig. 13. Wear behaviour over time at 200 °C and 400 °C in air (50 N, 15 Hz, 1.6 mm & 120 min).

If an oxidation-dominated wear mechanism is assumed, as for example described by Quinn [11], then an existing oxide layer from both contacting bodies is removed either by the increasing instability of the layer or by the shearing of the second body, which leads to wear. According to [42], a parabolic oxidation rate can be assumed for both materials, which corresponds to the following relationship:

$$\frac{dx}{dt} = \frac{k_p}{x} \tag{5}$$

where x is the oxide thickness, k_p is the parabolic rate constant and t is the time. Consequently, the oxidation rate of native surfaces is the fastest initially and then decreases with increasing oxide thickness as well as time [42]. The highest wear would therefore be expected at a high frequency and short time intervals between traverses, as the oxide layers forming are removed quickly at a high repetition rate. At slower frequencies, the oxidation rate is reduced by the oxide layer that has already formed, resulting in less oxide which is worn off as wear. However, the findings show an opposite trend, with lower wear at higher frequencies. For this reason, another dominant interaction is assumed in this study, which determines the wear behaviour.

As the displacement was also varied in addition to the frequency for comparable sliding speeds, its influence is analysed in more detail in the following. The displacement significantly influences the contact surface, and this results in different friction energy densities. However, a wear-reducing influence due to high friction energy densities is questionable, especially in the area of abrasion and oxidation, which is why this is excluded as a possible explanation.

Instead, it is assumed that the displacement has a significant effect on the particle movements and, above all, their ejection rates. The smaller the displacement, the closer one gets to the area of fretting or, in extreme cases, the partial slip area, which is mainly influenced by the supply of reactive gases [45,46]. With these small displacements, only a few wear particles are transported out of the contact area. This has a positive effect on the formation of the glaze layer in the high temperature region, and at lower temperatures wear-reducing effects are also known due to the formation of a particle bed as a third body [47–49]. The greater the displacement, the more particles are ejected from the contact area, resulting in an increase of wear. This theory of particle influence, which has also been postulated as a rate determining process in some publications concerning fretting [46,50,51], can be used to describe the measured wear behaviour.

Consequently, for the mathematical description of the dominant influencing factors, the displacement δ_0 with an approximately linear correlation with the wear volume V_{f/δ_0} is defined:

$$V_{f/\delta_0} \sim \delta_0 \tag{6}$$

Table 7
Determined model constants for time/sliding distance influence.

Constant	Value	Unit
$a_{t,200C}$	0.121	µm $s^{-0.714}$
$b_{t,200C}$	0.714	–
$a_{t,400C}$	0.068	µm $s^{-0.773}$
$b_{t,400C}$	0.773	–

3.4. Influence of sliding distance or test duration on the wear behaviour

Time and sliding distance were investigated as the next parameter, which are influencing the wear behaviour. A distinction is made between the wear regimes of abrasion and oxidation in the lower temperature range and glaze layer formation in the upper temperature range.

3.4.1. Abrasive & oxidative wear regime up to 500 °C

Comparatively high wear rates are observed in the lower temperature range, which enable a reliable evaluation of the built-in wear depth sensor of the test rig. This capacitive sensor measures the position change of the cylinder caused by the wear of both contact bodies to which the normal force is applied. The development of the system wear depth at 200 °C and 400 °C are shown in Fig. 13. They display a similar wear increase over time with a slightly falling rate after 45 - 60 min.

This time behaviour is best described by a power function with the test duration t or the sliding distance s and their corresponding constants a_s, b_s or a_t, b_t in the following form:

$$V_{s/t} \sim a_s\ s^{\,b_s}\ ,\quad a_t\ t^{\,b_t} \qquad \text{for} \quad T < T_{GL} \tag{7}$$

Many already established wear models, such as Archard's wear equation [10], Quinn's oxidation wear [11] or newer, application-specific models [4,6,46] assume linear behaviour. However, the results presented show a deflection of the time behaviour, therefore a more precise mathematical description was chosen. The model constants were determined for both curves and listed in Table 7. A coefficient of determination of 0.9974 was determined for 200 °C and 0.9952 for 400 °C, indicating a sufficiently accurate approximation.

3.4.2. Glaze layer wear regime above 600 °C

In the upper temperature range, which is characterised by low wear due to the glaze layer formation, it is more difficult to record the wear development. As the built-in wear depth measurement of the SRV cannot be used reliably at these low wear values in combination with the large thermal gradients, the established confocal microscope measurement was used. To enable repeated, precisely positioned mounting of the specimen between tests and analysis, the plates were equipped with marks. To measure the cylinder, the entire holder was dismounted instead of the specimen body, which also allows repeated precise positioning. This procedure made it possible to determine the wear evolution shown in Fig. 14.

The wear of the plate already shows high values in the first measurement after two minutes and fluctuates significantly over the entire duration of the test. This behaviour is attributed to the high porosity of the plate, which on the one hand is misinterpreted as wear and on the other hand can lead to high differences between repeated analysis even with slightly different measurement positions. As a result, the plate wear is not taken into account any further. The development of wear on the cylinder is far more interesting. Here, after an initial steep increase in wear, a linear behaviour sets in from approx. 15 min, which also correlates with the running-in behaviour of the friction coefficient. It is assumed that this initial phase is required to fully form the glaze layer and, in particular, to allow the Co_3O_4-rich and wear-reducing surface layer described by [5] to form on the mixed oxide

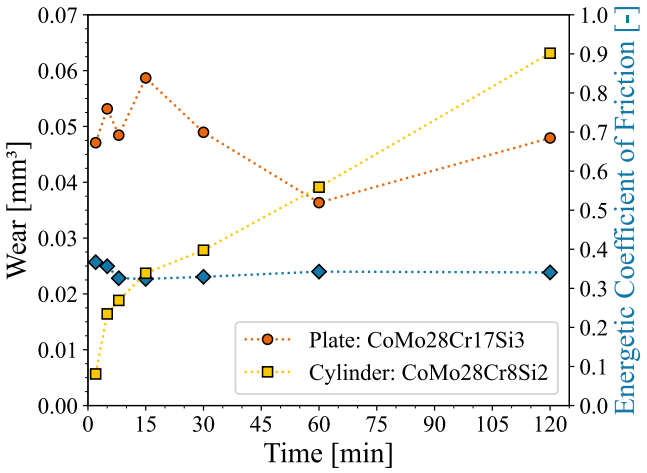

Fig. 14. Wear behaviour over time at 800 °C in air (50 N, 8 Hz, 3.2 mm & 120 min).

layer. The reduction of contact stress by an increased contact width after time is not seen as a dominant factor for the glaze layer formation, as different normal forces result in comparable wear volumes (Fig. 11). Accordingly, the relationship established in Eq. (8) can be extended to the entire investigated temperature range:

$$V_{s/t} \sim s, t \qquad \text{for} \quad T > T_{GL} \tag{8}$$

These results stand in clear contrast to the results of Dreano et al. [4–6,30], who investigated the formation of a glaze layer in a Co-based alloy under fretting in detail. They found evidence of stagnating wear as soon as the glaze layer has fully formed. This property was subsequently used as the basis for the postulated wear model. However, the results obtained here clearly show that a minimal wear rate must be expected although the glaze layer is fully formed. Only the different contact configurations could have led to these differences, as the proportion of ejected wear particles is marginal in the case of fretting, with the result that no change in wear could be detected. With the reversing experiments investigated here using a stroke of 1.6 mm, a significantly higher particle ejection must be expected, which leads to an increase in wear that was detectable using established analysis methods.

3.5. Influence of atmosphere

In the following section, the influence of the atmosphere on the wear and friction behaviour of the material pairing is presented and discussed. The interaction between temperature and atmosphere is discussed first and then the influence of varying atmospheric compositions is described.

3.5.1. Temperature dependent atmospheric effect

As the material pairing investigated is used in bearings of flaps or valves which operate in exhaust gas systems of combustion engines, the atmospheric effect of an idealised diesel exhaust gas was studied. The oxygen content of the synthetically generated exhaust gas atmosphere for these tests was 5 vol.% with approx. 15.2 vol.% CO_2 and is therefore comparable to the exhaust gas composition of a diesel engine in partial load conditions [52]. Fig. 15 compares the tribological test results in this atmosphere with the previously discussed results in ambient air. The wear of both contact bodies was summarised and plotted on a logarithmic scale for an easier identification of the differences.

In the lowest temperature range up to 300 °C, significantly higher wear values were detected in the $CO_2/N_2/O_2$-atmosphere than in air. The maximum difference occurs at room temperature and decreases with increasing temperature until comparable wear values were measured at 400 °C for both atmospheres. For this lowest temperature

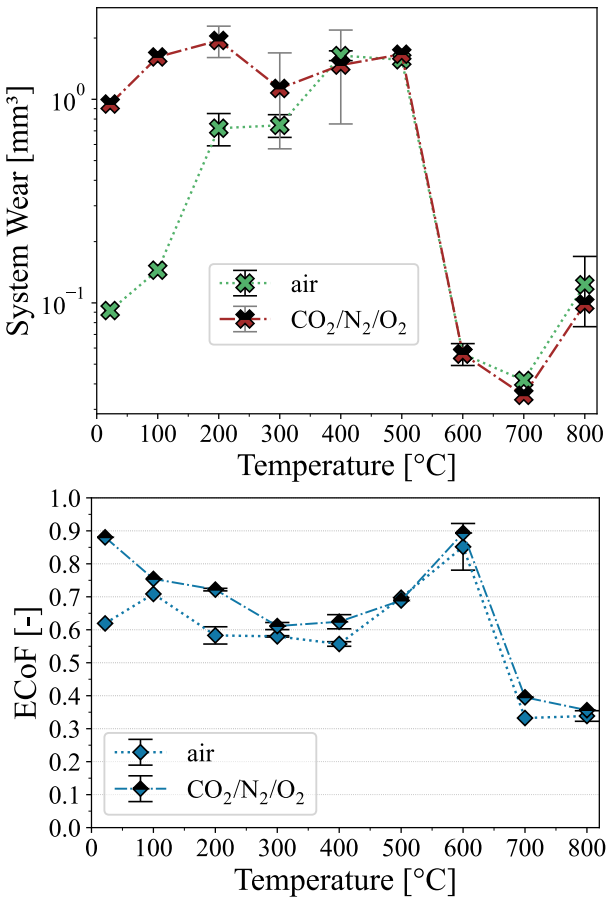

Fig. 15. Wear and friction results of isothermal tests in air and $CO_2/N_2/O_2$-atmosphere (50 N, 15 Hz, 1.6 mm, 120 min, 5 vol.% O_2).

range, differing levels of the energetic coefficient of friction were determined, with a higher friction by 0.1–0.25 in the $CO_2/N_2/O_2$-atmosphere (at 100 °C in air an outlier can be assumed, as already discussed). At 400 °C and higher no significant differences in wear were observed between the atmospheres.

To illustrate the difference in friction behaviour for the lowest temperature range, friction curve examples of the corresponding atmospheres at 200 °C are shown in Fig. 16. The test in air displays a slight but constant decrease of the friction coefficient between 0.65 and 0.55 over time. This continuous friction behaviour can be attributed to the occurring abrasive wear mechanism. In contrast, in the $CO_2/N_2/O_2$-atmosphere, a significantly more fluctuating behaviour with many friction peaks was recorded, which reached high values between 0.65 and 0.85 in the second half of the test. This indicates a change in the dominant tribological mechanism, leading to strong friction fluctuations in the case of a high level of adhesion.

To clarify this atmosphere-related change of the wear mechanisms, the wear surfaces and height information of the plates are shown in Fig. 17 and the wear surfaces of the cylinders in Fig. 18. When comparing the plates, the high number of adhering wear particles in the $CO_2/N_2/O_2$-atmosphere is remarkable, which looks at first like a smoothed, slightly plastically deformed, viscous liquid and completely covers the pores which are visible for the test in air. Furthermore, the significantly larger wear depth in the $CO_2/N_2/O_2$-atmosphere can be identified from the height information, which shows irregular and large grooves with chipping of the porous material in the centre. In contrast, the plate wears only minimally in air. A atmosphere related wear shift from cylinder to plate can be summarised. Significant atmospheric differences can also be recognised for the wear surfaces of

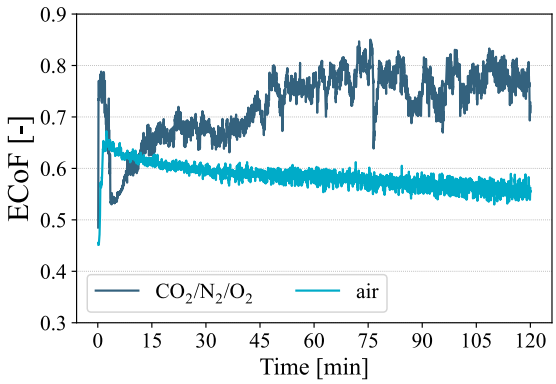

Fig. 16. Friction behaviour over time of isothermal tests in air and $CO_2/N_2/O_2$-atmosphere at 200 °C (50 N, 15 Hz, 1.6 mm, 120 min, 5 vol.% O_2).

the cylinders. The cylinder tested in the $CO_2/N_2/O_2$-atmosphere shows a large amount of adhering material flakes from the counter body, which become electrostatically charged in the SEM due to the higher oxide content and are therefore were displayed in a lighter colour. Whereas in air, mainly abrasive grooves and small, adhering, oxidised and therefore darker wear particles can be identified.

Consequently, a shift of the dominant wear mechanisms takes place in the low temperature range up to 300 °C due to atmospheric changes. Abrasion, which dominates in air and leads to one-sided wear on the cylinder, is replaced by adhesive material transfer from the porous plate onto the cylinder in the $CO_2/N_2/O_2$-atmosphere. This is accompanied by a severe increase in friction in the $CO_2/N_2/O_2$-atmosphere and the increased adhesive properties of the wear particles lead to a significant debris coverage of the plate.

These adhering wear particles, which even fill the pores of the plate material, were analysed in more detail using an FIB cross-section. This is represented in Fig. 19 and shows on the left side the round edge of a deposited material particle and in the centre the darker coloured wear particles, which fill a cavity of the sprayed layer on the plate. In addition to isolated inclusions, cracks can be seen between some of the adhering wear particles, allowing conclusions to be drawn about their shape and indicating not only agglomeration and compaction but also plastic deformation due to the tribological load.

To investigate a possible tribochemical influence of the atmosphere, XPS depth profiles were determined for these plates tested at 200 °C, and are shown in Fig. 20. The significantly higher oxygen and carbon content, the significant decrease of the cobalt fraction and a slightly lower molybdenum fraction in the $CO_2/N_2/O_2$-atmosphere compared to air are distinctive. The higher oxygen and lower cobalt content are attributed to the previously described extensive adherence of oxidised wear particles and are therefore not unexpected. However, the higher carbon content is more interesting, because it is also present at depths of 200–500 nm which argues against possible residues from sample cleaning. The detailed evaluation of the XPS analysis data revealed a clear shift of the C1s peak to lower binding energies (Fig. 21), which are characteristic of carbides. However, the energy distributions of the metals do not allow any conclusions about possible carbide compounds, as the relevant binding energies correspond to those of the oxides. Further systematic EDX analyses of adhering wear particles (see supplementary data) also revealed a higher carbon content, which was accompanied by a higher chromium content in the $CO_2/N_2/O_2$-atmosphere compared to air. Moreover, the positioning of the three possible metals within the electrochemical series (Mo −0.2 V [53]; Co −0.282 V [54]; Cr −0.76/−0.89 V [54,55]) also indicates the highest tendency for chromium to release electrons. As a result, a tribochemical reaction of CO_2 from the atmosphere with chromium is assumed, which results in the generation of chromium carbides. The formed, hard

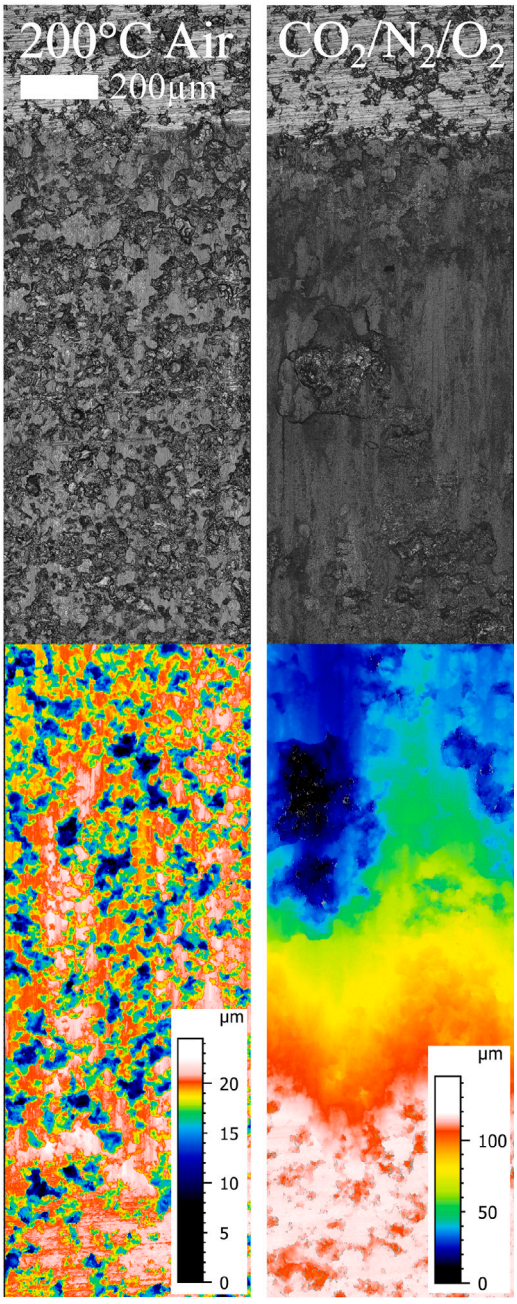

Fig. 17. Worn surfaces and height information of plates (CoMo28Cr17Si3 HVOF-plating) after isothermal tests in air and $CO_2/N_2/O_2$-atmosphere at 200 °C (50 N, 15 Hz, 1.6 mm, 120 min, 5 vol.% O_2); both images have the same scale.

chromium carbides act as an abrasive medium, adhering to the softer cylinder material and increasing wear on the plate.

The atmosphere-related increase in friction and wear at the lowest temperature range can therefore be attributed to the mechanism change from abrasion to adhesion, which is correlated to a tribochemical reaction with the CO_2 content of the atmosphere and the slower oxidation. A formation of chromium carbides due to the tribochemical reaction is assumed. Caused by the adhesive material transfer onto the cylinder, as well as adhering abrasive wear particles, mainly the disc wears in the $CO_2/N_2/O_2$-atmosphere.

In the high temperature range of 700 - 800 °C no influence of the atmospheric variation on the glaze layer formation was observed. It is assumed that, based on the previously discussed TEM analyses of the

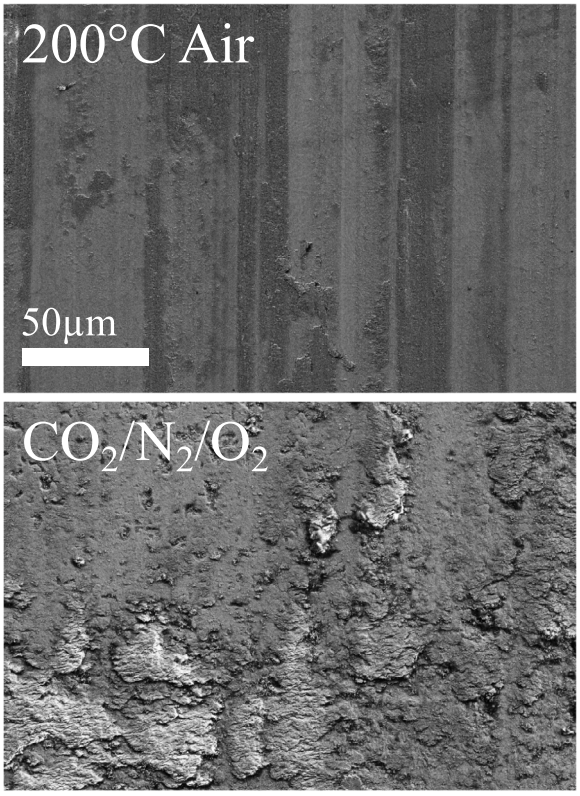

Fig. 18. Details of worn cylinder surfaces (CoMo28Cr8Si2) after isothermal tests in air and $CO_2/N_2/O_2$-atmosphere at 200 °C (50 N, 15 Hz, 1.6 mm, 120 min, 5 vol.% O_2).

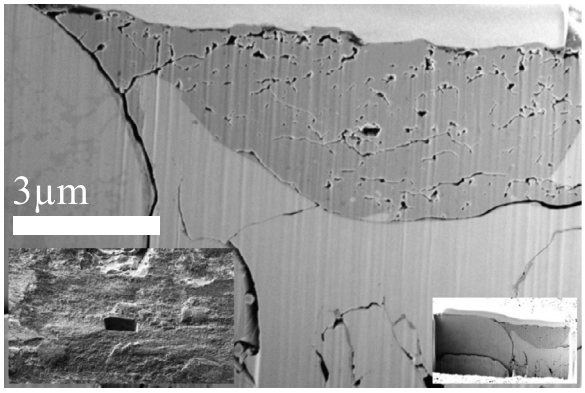

Fig. 19. FIB-cross section of adhering material in a pore of the plate (CoMo28Cr17Si3 HVOF-plating on 1.4713) after isothermal tests in $CO_2/N_2/O_2$-atmosphere at 200 °C (50 N, 15 Hz, 1.6 mm, 120 min, 5 vol.% O_2).

wear particles, the debris is already in an oxidised state even in the $CO_2/N_2/O_2$-atmosphere below 600 °C. However, the thermal energy required for the sintering process of the glaze layer is only achieved for tests at 600 °C, therefore no atmosphere-related influence applies.

These results on the influence of the atmosphere on an unlubricated high-temperature tribological system are consistent with the findings published in [20] for an iron-based material pairing. Here, as well, atmospheric changes in wear behaviour were only detected in the lowest temperature range. The oxidation of the material-specific graphite fraction, which was further slowed down by the lower oxygen partial pressure, led to an improvement in the wear-reducing effect of the graphite and resulted in slightly lower wear. In the high temperature range, the wear-reducing glaze layer formation based on Fe_2O_3 was not affected by the tested atmospheres either. Comparable findings

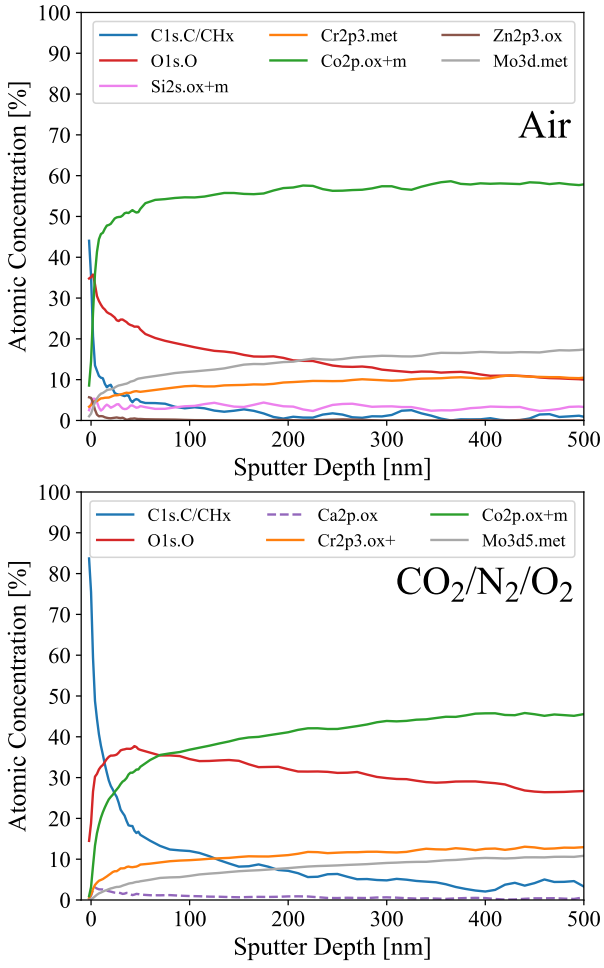

Fig. 20. XPS depth profiles of plates tested at 200 °C in air and in $CO_2/N_2/O_2$-atmosphere (50 N, 15 Hz, 1.6 mm, 120 min, 5 vol.% O_2).

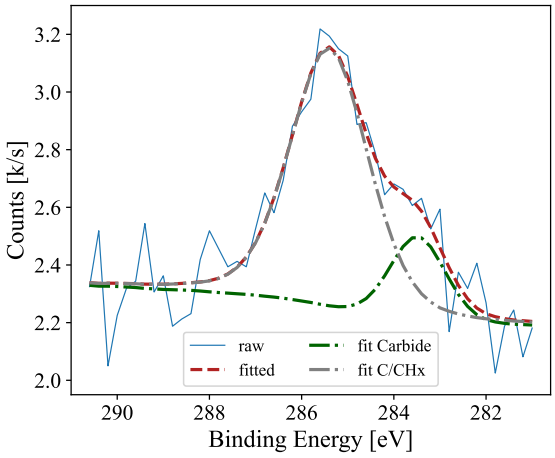

Fig. 21. XPS results of the C1s peak in 80 nm depth measured at a plate tested at 200 °C in $CO_2/N_2/O_2$-atmosphere (50 N, 15 Hz, 1.6 mm, 120 min, 5 vol.% O_2).

were also made by Jiang et al. [13], who investigated the temperature- and atmosphere-dependent wear behaviour of a nickel-based alloy. In the lower temperature range, atmospheric changes had a strong effect on wear, while decreasing oxygen content significantly increased wear due to rising adhesion. In the upper temperature range, where glaze layer formation occurs, an atmospheric effect could only be detected at

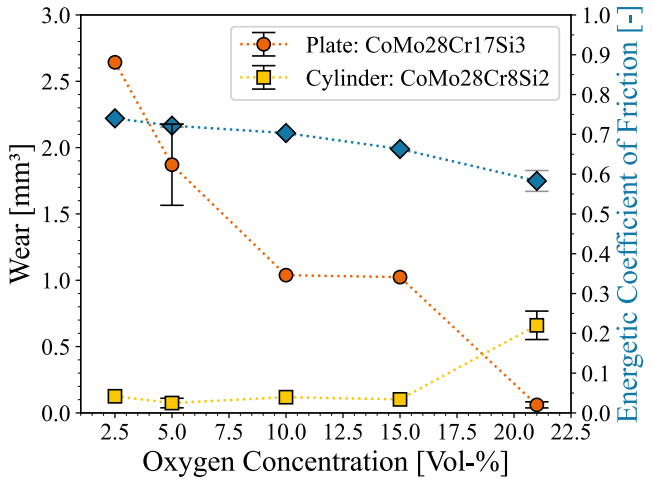

Fig. 22. Tribologiac results of isothermal tests at 200 °C in different atmospheres (50 N, 15 Hz, 1.6 mm & 120 min).

oxygen contents below 1.5 vol.% in an argon atmosphere. In the present study, however, the oxygen content was at least 5 vol.% for comparable operating conditions to exhaust gas systems, where no changes in the formation of the glaze layer were observed.

Further studies investigating the influence of minimally oxygen-containing atmospheres on wear behaviour at high temperatures are unknown. For oxygen-free inert gas atmospheres, however, a strong increase in wear due to the lack of an oxide layer at high temperatures has already been repeatedly demonstrated [18,19].

An atmosphere-induced change of tribochemical reactions was also demonstrated by Velkavrh et al. [17,35], who carried out experiments in different inert gases. They demonstrated impressively that the chemical inertness of the atmospheres has a direct influence on the tribochemical products and thus on friction and wear. For tests in a pure CO_2-atmosphere, CO-containing coatings were determined with a significant decrease in stability when the temperature was increased to 200 °C.

Empirically, the temperature-dependent atmospheric influence on wear behaviour can be described with the following exponential function:

$$\frac{V_{CO_2/N_2/O_2}}{V_{air}} \sim e^{-k_T\ T} \qquad (9)$$

with $k_{T,I}$ for $T < T_{GL}$

Here $V_{CO_2/N_2/O_2}$ corresponds to the wear volume in the CO_2/N_2 /O_2-atmosphere, V_{air} to the wear volume in ambient air and $k_T(T)$ is a constant.

3.5.2. Composition dependent atmospheric effect

The following section details the influence of the atmospheric composition on the tribological material behaviour. For this purpose, tests were carried out at 200 °C with different oxygen contents as well as mixing ratios with the CO_2-N_2 cylinder gas and the results are visualised in Fig. 22. The values shown at 5 vol.% oxygen correspond to the results already presented and discussed in the previous section and those at 21 vol.% correspond to the results in ambient air.

A clear increase of the wear volume with decreasing oxygen content or increasing CO_2 content has been demonstrated for the plate. This trend is accompanied by a rising energetic coefficient of friction, which, as previously discussed, can be attributed to a mechanism change from abrasion to adhesive material transfer. As a result of the mechanism change, a shift of the dominant wear component occurs, from the cylinder in air to the plate in the $CO_2/N_2/O_2$-atmosphere. Furthermore, the results show that a reduction from air (20.9 vol.%) to 15 vol.% oxygen already leads to this mechanism change and thus to a shift in the wear proportions, but the total wear of the system initially rises only slightly.

Only by Jiang et al. [13], the atmospheric composition was investigated in depth as an influencing factor on tribological material behaviour. They used a nickel-based alloy as a like-on-like pairing for their studies and transferred the results into a particle-based wear model. For low temperatures around 150 °C and a decreasing oxygen partial pressure of 21 - 2.5 kPa, their model also predicts an increase in wear volume, which is explained by an increase of adhesion. Mathematically, this is taken into account by an increase in particle size and a decrease in the number of wear particles with lower oxygen partial pressures in the wear model and is therefore only partially comparable. However, the atmospheric shift of the wear mechanisms towards adhesion was also demonstrated by Qiu et al. [56] for chromium steels at low temperatures, although only tests in air and pure CO_2 and N_2 were carried out. A mathematical description was not provided.

However, comparable findings were obtained in studies on oxidation kinetics under different atmospheric compositions. For example, a root-shaped correlation of the parabolic oxidation rate with the oxygen partial pressure was determined for pure cobalt by Mrowec et al. [57]. The determined values of the exponent and other literature data listed vary between 1/2.5 - 1/3.4, whereby these values were identified at temperatures around 950 °C and show an increasing tendency with rising temperatures. Przybylski et al. [58] also demonstrated that the chromium content of a cobalt alloy has a significant influence on the oxidation kinetics due to the high oxidation tendency. Again, exponents between 1/2 - 1/2.6 were found for the correlation of the oxidation rate with the oxygen partial pressure at temperatures of 1000 °C. More recent oxidation studies by Peng et al. [42], which analysed the investigated alloy, conclude that the initial oxidation behaviour is significantly faster than a parabolic law.

In the lower temperature range of this material pairing, the abrasion of the cylinder dominates the wear behaviour in air. As already discussed repeatedly, an oxidative-abrasive wear equation based on [4] and [11] is suitable for describing this behaviour. Following this model, higher temperatures, normal forces, etc. lead to faster oxidation of the base material and result in a faster formation and subsequent erosion of this oxide layer with consequently higher wear. However, if the oxidation rate of the material decreases due to the change to the atmosphere, the oxide layer formation is much slower. Due to the increasing number of nascent surface areas, the proportion of adhesive wear increases and results in significantly higher overall wear for oxygen-reduced atmospheres. The previously discussed findings on oxygen-dependent oxidation kinetics are therefore consistent with the experimental results, their interpretation and the subsequent model of understanding. Mathematically, the correlation of the total wear volume $V_{\varphi_{O_2}}$ with the oxygen content of the surrounding atmosphere φ_{O_2} at 200 °C can be described by a hyperbolic function with an exponent of −1/2:

$$V_{\varphi_{O_2}} \sim \frac{1}{\sqrt{\varphi_{O_2}}} \qquad (10)$$

4. Conclusion

This publication addresses the most important influencing factors (temperature, normal force, displacement or frequency, sliding distance and atmosphere) of an unlubricated tribological system which is exposed to high thermal loads in exhaust systems of internal combustion engines. The objective is to further deepen the understanding of these fundamental tribological mechanisms such as abrasion, oxidation or glaze layer formation and to enable these findings to be transferred from the investigated Co-based alloys (CoMo28Cr17Si3 vs. CoMo28Cr8Si2) to other material systems by mathematically correlating the influencing factors with the resulting wear. The most important findings are summarised in Fig. 23 and described below:

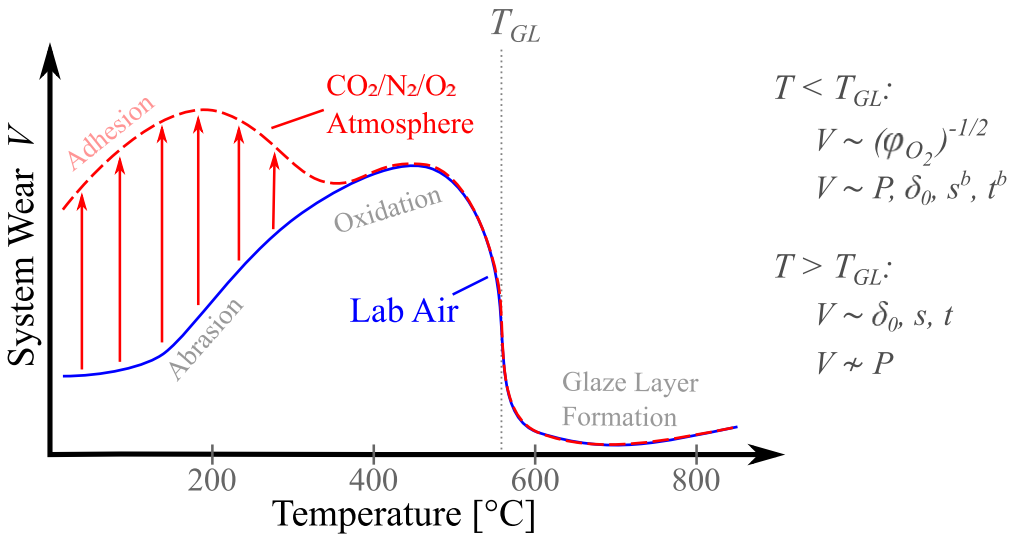

Fig. 23. Temperature and atmosphere dependent wear behaviour and other empirical correlations regarding the oxygen content of the surrounding atmosphere φ_{O_2}, normal force P, stroke δ_0, and test duration t respectively sliding distance s.

- **Influence of temperature:** The main factor influencing tribological material behaviour can be subdivided in three temperature ranges. Up to 300 °C the abrasion of the cylinder is dominant and between 400 - 500 °C the increased oxidation and slight adhesion of the wear particles leads to high wear of the plate. From 600 - 800 °C the formation of a friction- and wear-reducing glaze layer sets in. As the wear particles have similar chemical compositions, structures and a homogeneous element distribution at different test temperatures, the thermal activation of the tribologically supported sintering process of these particles is the dominant influencing factor on the formation of the glaze layer. The thermally induced increase of wear can be described mathematically for both temperatures below and above the glaze layer formation temperature (T_{GL}) by an Arrhenius correlation with different energy barriers and factors.
- **Influence of normal force:** For the abrasive/oxidative wear regime ($T < T_{GL}$), the wear increases almost linearly with rising normal force. In the glaze layer regime ($T > T_{GL}$), no influence of the normal force on the wear behaviour was observed.
- **Influence of displacement/frequency:** In addition to the tribologically induced local temperature increase at higher frequencies, the displacement also has a significant influence on the wear behaviour. It affects the particle transport in the contact zone and especially the particle ejection. With a smaller displacement, wear decreases linearly for all temperature ranges, as a higher particle ejection hinders a third body formation at low temperatures ($T < T_{GL}$) or has a negative effect on the continuous sintering process in the glaze layer regime ($T > T_{GL}$).
- **Influence of sliding distance/test duration:** A power law describes the observed time behaviour of the system wear depth in the abrasive/oxidative wear regime ($T < T_{GL}$). After running-in and the formation of a glaze layer ($T > T_{GL}$), a approximately linear increase in wear with increasing sliding distance was demonstrated and attributed to a continuous particle ejection. This is in clear contrast to previously postulated findings of complete wear prevention by a glaze layer [5,6,12,13,30].
- **Temperature dependent atmospheric effect:** The influence of a diesel exhaust gas-like atmosphere instead of ambient air leads to a significant increase in friction and wear. This is related to a mechanism change from abrasive to adhesive wear in the lower temperature regime ($T < T_{GL}$). A tribochemical reaction with the CO_2 of the exhaust gas-like atmosphere, along with a slower oxidation reaction, is considered to be the cause of the increased adhesion tendency. The carbides produced by this reaction were detected using XPS. At high temperatures ($T > T_{GL}$) no atmosphere dependent influence of the glaze layer formation can be observed, which is attributed to already fully oxidised wear particles at these temperatures.
- **Composition dependent atmospheric effect:** A hyperbolic increase of wear with decreasing oxygen content was determined for the abrasive/oxidative wear regime ($T < T_{GL}$). The underlying mechanism change towards adhesion can be set in relation to the exponential oxygen dependence of the oxidation rate, which thus significantly determines the wear behaviour.

CRediT authorship contribution statement

Tobias König: Writing – original draft, Methodology, Investigation, Conceptualization. **Eduard Wolf:** Investigation. **Philipp Daum:** Writing – review & editing, Investigation. **Dominik Kürten:** Writing – review & editing, Supervision, Methodology, Funding acquisition, Conceptualization. **Andreas Kailer:** Writing – review & editing, Supervision, Methodology, Funding acquisition, Conceptualization. **Martin Dienwiebel:** Writing – review & editing, Supervision, Funding acquisition, Conceptualization.

Declaration of competing interest

The authors declare the following financial interests/personal relationships which may be considered as potential competing interests: Tobias Koenig reports financial support was provided by Federal Ministry for Economic Affairs and Climate Action of the Federal Republic of Germany. Tobias Koenig reports equipment, drugs, or supplies was provided by Research Association for Combustion Engines. If there are other authors, they declare that they have no known competing financial interests or personal relationships that could have appeared to influence the work reported in this paper.

Acknowledgements

We are grateful to Martin Peterlechner from the Laboratory for Electron Microscopy (LEM) at the Karlsruhe Institute of Technology (KIT) for performing the transmission electron microscopy measurements. We acknowledge funding from the Federal Ministry for Economic Affairs and Climate Action of the Federal Republic of Germany

under grant agreement no. 21253 N. The authors are grateful for the support of AiF (Arbeitsgemeinschaft industrieller Forschungsvereinigungen) within the program for sponsorship by Industrial Joint Research (IGF) of the Federal Ministry for Economic Affairs and Climate Action (BMWK) based on an enactment of the German Parliament. The authors would also like to thank the Forschungsvereinigung Verbrennungsmotoren FVV e.V. for their appreciated technical support.

Appendix A. Supplementary data

Supplementary material related to this article can be found online at https://doi.org/10.1016/j.wear.2025.205758.

Data availability

Data will be made available on request.

References

[1] P.J. Blau, Elevated-temperature tribology of metallic materials, Tribol. Int. 43 (7) (2010) 1203–1208.
[2] P.J. Blau, Fifty years of research on the wear of metals, Tribol. Int. 30 (5) (1997) 321–331.
[3] A. Renz, B. Prakash, J. Hardell, O. Lehmann, High-temperature sliding wear behaviour of Stellite®12 and Tribaloy®T400, Wear 402–403 (2018) 148–159.
[4] A. Dréano, S. Fouvry, G. Guillonneau, A tribo-oxidation abrasive wear model to quantify the wear rate of a cobalt-based alloy subjected to fretting in low-to-medium temperature conditions, Tribol. Int. 125 (2018) 128–140.
[5] A. Dreano, S. Fouvry, S. Sao-Joao, J. Galipaud, G. Guillonneau, The formation of a cobalt-based glaze layer at high temperature: A layered structure, Wear 440–441 (2019) 203101.
[6] A. Dreano, S. Fouvry, G. Guillonneau, Understanding and formalization of the fretting-wear behavior of a cobalt-based alloy at high temperature, Wear 452–453 (2020) 203297.
[7] E.M. do Nascimento, L.M. do Amaral, A.S.C. D'Oliveira, Characterization and wear of oxides formed on CoCrMoSi alloy coatings, Surf. Coat. Technol. 332 (2017) 408–413.
[8] R. McCarron, D. Stewart, P. Shipway, D. Dini, Sliding wear analysis of cobalt based alloys in nuclear reactor conditions, Wear 376–377 (2017) 1489–1501.
[9] P. Cross, G. Limbert, D. Stewart, R. Wood, Ratcheting wear of a cobalt-chromium alloy during reciprocated self-mated dry sliding, Wear 426–427 (2019) 1142–1151.
[10] J.F. Archard, Contact and rubbing of flat surfaces, J. Appl. Phys. 24 (8) (1953) 981–988.
[11] T. Quinn, Oxidational wear, Wear 18 (5) (1971) 413–419.
[12] F.H. Stott, The role of oxidation in the wear of alloys, Tribol. Int. 31 (1–3) (1998) 61–71.
[13] J. Jiang, F.H. Stott, M.M. Stack, A generic model for dry sliding wear of metals at elevated temperatures, Wear 256 (9–10) (2004) 973–985.
[14] T. Quinn, Oxidational wear modelling part III. The effects of speed and elevated temperatures, Wear 216 (2) (1998) 262–275.
[15] X. Jin, P.H. Shipway, W. Sun, The role of temperature and frequency on fretting wear of a like-on-like stainless steel contact, Tribol. Lett. 65 (3) (2017).
[16] C. Zhang, R.W. Neu, Temperature-frequency wear mechanism maps for a heat-resistant austenitic stainless steel, Wear 522 (2023) 204844.
[17] I. Velkavrh, F. Ausserer, S. Klien, J. Brenner, P. Forêt, A. Diem, The effect of gaseous atmospheres on friction and wear of steel–steel contacts, Tribol. Int. 79 (2014) 99–110.
[18] M.S. Rahman, J. Ding, A. Beheshti, X. Zhang, A.A. Polycarpou, Helium tribology of inconel 617 at elevated temperatures up to 950°C: Parametric study, Nucl. Sci. Eng. 193 (9) (2019) 998–1012.
[19] A. Ahmadi, F. Sadeghi, S. Shaffer, In-situ friction and fretting wear measurements of Inconel 617 at elevated temperatures, Wear 410–411 (2018) 110–118.
[20] T. König, T. Kimpel, D. Kürten, A. Kailer, M. Dienwiebel, Influence of atmospheres on the friction and wear of cast iron against chromium plated steel at high temperatures, Wear 522 (2023) 204695.
[21] R.D. Schmidt, D.P. Ferriss, New materials resistant to wear and corrosion to 1000°C, Wear 32 (3) (1975) 279–289.
[22] Deloro Wear Solutions GmbH, Technical Data Tribaloy T400, Koblenz, Germany, 2023, URL: https://www.deloro.com/fileadmin/users/redakteur/006_Downloads/Data_Sheets/Deloro_MDS_Tribaloy400_rev00.pdf.
[23] Deloro Wear Solutions GmbH, Technical Data Tribaloy T800, Koblenz, Germany, 2023, URL: https://www.deloro.com/fileadmin/users/redakteur/006_Downloads/Data_Sheets/Deloro_MDS_Tribaloy800_rev00.pdf.
[24] S. Fouvry, P. Duó, P. Perruchaut, A quantitative approach of Ti–6Al–4V fretting damage: friction, wear and crack nucleation, Wear 257 (9–10) (2004) 916–929.
[25] I. Llavori, A. Zabala, A. Aginagalde, W. Tato, J.J. Ayerdi, X. Gómez, Critical analysis of coefficient of friction derivation methods for fretting under gross slip regime, Tribol. Int. 143 (2020) 105988.
[26] S. Fouvry, R. Merhej, Introduction of a power law formulation to quantify the contact size effects on friction and wear responses of dry oscillating sliding contacts: Application to a chromium steel interface, Wear 301 (1–2) (2013) 34–46.
[27] X. Jin, W. Sun, P.H. Shipway, Derivation of a wear scar geometry-independent coefficient of friction from fretting loops exhibiting non-Coulomb frictional behaviour, Tribol. Int. 102 (2016) 561–568.
[28] ASTM Committee G02, Guide for Determining Friction Energy Dissipation in Reciprocating Tribosystems: G0203-10, ASTM International, West Conshohocken, USA, 2016.
[29] B. Rivas-Murias, V. Salgueiriño, Thermodynamic CoO-Co 3 O 4 crossover using Raman spectroscopy in magnetic octahedron-shaped nanocrystals, J. Raman Spectrosc. 48 (6) (2017) 837–841.
[30] A. Dreano, S. Fouvry, G. Guillonneau, A combined friction energy and tribo-oxidation formulation to describe the high temperature fretting wear response of a cobalt-based alloy, Wear 426–427 (2019) 712–724.
[31] A. Korashy, H. Attia, V. Thomson, S. Oskooei, Characterization of fretting wear of cobalt-based superalloys at high temperature for aero-engine combustor components, Wear 330–331 (2015) 327–337.
[32] R.T. Foley, M.B. Peterson, C. Zapf, Frictional characteristics of cobalt, nickel, and iron as influenced by their surface oxide films, A S L E Trans. 6 (1) (1963) 29–39.
[33] S.R. Pearson, P.H. Shipway, J.O. Abere, R. Hewitt, The effect of temperature on wear and friction of a high strength steel in fretting, Wear 303 (1–2) (2013) 622–631.
[34] F.H. Stott, High-temperature sliding wear of metals, Tribol. Int. 35 (8) (2002) 489–495.
[35] I. Velkavrh, F. Ausserer, S. Klien, J. Voyer, A. Ristow, J. Brenner, P. Forêt, A. Diem, The influence of temperature on friction and wear of unlubricated steel/steel contacts in different gaseous atmospheres, Tribol. Int. 98 (2016) 155–171.
[36] C. Zhang, R.W. Neu, Understanding the role of glaze layer with aligned images from multiple surface characterization techniques, Wear 477 (2021) 203837.
[37] M.N. Rahaman, Sintering of Ceramics, CRC Press, Boca Raton, USA, 2007, pp. 4–6.
[38] H. Kato, K. Komai, Tribofilm formation and mild wear by tribo-sintering of nanometer-sized oxide particles on rubbing steel surfaces, Wear 262 (1–2) (2007) 36–41.
[39] M.N. Rahaman, Ceramic Processing, second ed., CRC Press, Boca Raton, USA, 2017, p. 388.
[40] C. Rynio, H. Hattendorf, J. Klöwer, G. Eggeler, The evolution of tribolayers during high temperature sliding wear, Wear 315 (1–2) (2014) 1–10.
[41] W. Xu, R. Liu, P.C. Patnaik, M.X. Yao, X.J. Wu, Mechanical and tribological properties of newly developed tribaloy alloys, Mater. Sci. Eng. A 452–453 (2007) 427–436.
[42] J. Peng, X. Fang, V. Marx, U. Jasnau, M. Palm, Isothermal oxidation behavior of TribaloyTM T400 and T800, Npj Mater. Degrad. 2 (1) (2018) 0–7.
[43] I.C. Grigorescu, Y. Gonzalez, O. Rodrigues, Y. de Vita, Tribological behaviour of electrochemically deposited coatings for shaft restoration, Surf. Coat. Technol. 76–77 (1995) 604–608.
[44] H. Kato, Effects of supply of fine oxide particles onto rubbing steel surfaces on severe–mild wear transition and oxide film formation, Tribol. Int. 41 (8) (2008) 735–742.
[45] S. Baydoun, P. Arnaud, S. Fouvry, Modelling adhesive wear extension in fretting interfaces: An advection-dispersion-reaction contact oxygenation approach, Tribol. Int. 151 (2020) 106490.
[46] P.H. Shipway, A.M. Kirk, C.J. Bennett, T. Zhu, Understanding and modelling wear rates and mechanisms in fretting via the concept of rate-determining processes - Contact oxygenation, debris formation and debris ejection, Wear 486–487 (2021) 204066.
[47] M. Godet, Third-bodies in tribology, Wear 136 (1) (1990) 29–45.
[48] J. Hintikka, A. Lehtovaara, A. Mäntylä, Third particle ejection effects on wear with quenched and tempered steel fretting contact, Tribol. Trans. 60 (1) (2017) 70–78.
[49] S. Baydoun, S. Fouvry, S. Descartes, Modeling contact size effect on fretting wear: a combined contact oxygenation - third body approach, Wear 488–489 (2022) 204168.
[50] T. Zhu, P.H. Shipway, W. Sun, The dependence of wear rate on wear scar size in fretting; the role of debris (third body) expulsion from the contact, Wear 440–441 (2019) 203081.
[51] T. Zhu, C.J. Bennett, P.H. Shipway, Debris expulsion as a rate determining process in fretting – The effect of slip amplitude on debris expulsion behaviour and rates, Wear 523 (2023) 204818.
[52] G.P. Merker, Grundlagen Verbrennungsmotoren: Funktionsweise, Simulation, Messtechnik, seventh ed., in: ATZ/MTZ-Fachbuch Ser, Springer Fachmedien Wiesbaden GmbH, Wiesbaden, 2014, p. 472.

[53] W.M. Haynes, CRC Handbook of Chemistry and Physics, ninety third ed., CRC and Taylor & Francis, Boca Raton, USA and London, 2012, pp. 5–84.
[54] D.C. Harris, G. Werner, T. Werner, Lehrbuch der Quantitativen Analyse, eight ed., Springer, Berlin, Heidelberg, 2014, pp. 907–917.
[55] T. Pearson, S. Handy, R.L. Forst, Elektrochemische Untersuchungen zum Korrosionsmechanismus dekorativer Chromoberflächen durch Calciumchlorid, Galvanotechnik (08) (2009) 1736.
[56] M. Qiu, L. Chen, Tribological characteristics of chromium steels in three various atmospheres under high-speed conditions, Wear 268 (11–12) (2010) 1342–1346.
[57] S. Mrowec, K. Przybylski, Oxidation of cobalt at high temperature, Oxid. Met. 11 (6) (1977) 365–381.
[58] K. Przybylski, D. Szwagierczak, Kinetics and mechanism of high-temperature oxidation of dilute cobalt-chromium alloys, Oxid. Met. 17 (3–4) (1982) 267–295.